Combustion Science and Technology

ISSN: 0010-2202 (Print) 1563-521X (Online) Journal homepage: www.tandfonline.com/journals/gcst20

Three-Dimensional Numerical Simulation of a Rotating Detonation Engine: Effects of the Throat of a Converging-Diverging Nozzle on Engine Performance

Seiichiro Eto, Nobuyuki Tsuboi, Takayuki Kojima & A. Koichi Hayashi

To cite this article: Seiichiro Eto, Nobuyuki Tsuboi, Takayuki Kojima & A. Koichi Hayashi (2016) Three-Dimensional Numerical Simulation of a Rotating Detonation Engine: Effects of the Throat of a Converging-Diverging Nozzle on Engine Performance, Combustion Science and Technology, 188:11-12, 2105-2116, DOI: 10.1080/00102202.2016.1213990

To link to this article: https://doi.org/10.1080/00102202.2016.1213990

COMBUSTION SCIENCE AND TECHNOLOGY
2016, VOL. 188, NOS. 11–12, 2105–2116
http://dx.doi.org/10.1080/00102202.2016.1213990

Taylor & Francis
Taylor & Francis Group

Three-Dimensional Numerical Simulation of a Rotating Detonation Engine: Effects of the Throat of a Converging-Diverging Nozzle on Engine Performance

Seiichiro Eto[a], Nobuyuki Tsuboi[b], Takayuki Kojima[c], and A. Koichi Hayashi[d]

[a]Department of Mechanical and Control Engineering, Kyushu Institute of Technology, Fukuoka, Japan; [b]Department of Mechanical and Control Engineering, Faculty of Engineering, Kyushu Institute of Technology, Fukuoka, Japan; [c]Japan Aerospace Exploration Agency, Chofu, Tokyo, Japan; [d]Development of Mechanical Engineering, Aoyama Gakuin University, Sagamihara, Kanagawa, Japan

ABSTRACT

The effect of a converging-diverging nozzle on the performance of a rotating detonation engine was estimated using three-dimensional numerical simulations with a detailed chemical reaction model. The nozzle in this article is composed of a long constant cross section, a short converging section, and a diverging section. The expansion area ratios of nozzles A and B in this article are 2.0 and 1.89, respectively. The periodic exhaust oscillation due to rotating detonation is considerably reduced by nozzle A. The variation of the time-averaged pressure is approximately 0.0048 MPa and the ratio to the time-averaged value is 1.3%. For nozzle B, the variation in pressure is approximately 0.018 MPa, and the ratio to the time-averaged value is 5%. The specific impulse of nozzle A increases by approximately 11 s (3.8%) compared with the value of nozzle B.

ARTICLE HISTORY
Received 31 October 2015
Revised 20 May 2016
Accepted 20 May 2016

KEYWORDS
Detonation engine;
Numerical simulation;
Shock wave

Introduction

Detonation is a shock-induced combustion wave that propagates through a reactive mixture. Detonation has been investigated for safety engineering. A pulse detonation engine (PDE) is a constant-volume-like combustion engine with a supersonic detonation wave. PDEs have recently been recognized as a new propulsion system for supersonic transportation. Detonation engines have a better theoretical thermal efficiency than conventional constant-pressure combustion engines (Wolanski, 2013). PDEs provide better efficiency than ramjet engines in terms of the fuel-based specific impulses (Ispf); however, the thrust under high frequency decreases because of the pulsed-flow operation (Wolanski, 2013).

Recent studies about propulsion using detonation focus on the rotating detonation engine (RDE), which obtains continuous thrust by using a rotating detonation in a coaxial chamber. The continuous thrust force of the RDE is most notably different from that of

CONTACT Seiichiro Eto p344111s@mail.kyutech.jp Department of Mechanical and Control Engineering, Kyushu Institute of Technology, 1-1 Sensuicho, Tobata, Kitakyushu, Fukuoka 804-8550, Japan.

Color versions of one or more of the figures in the article can be found online at www.tandfonline.com/gcst.

the PDE. The RDE was first studied by Voitsekhovsky (1959), who investigated the spin detonation that propagated in the cylinder. Nicholls et al. (1966) concluded that there were many tasks to inject the combustible gas mixture to stabilize the rotating detonation. Zhdan et al. (2007) studied the continuous rotating detonation phenomena using experimental and numerical approaches and estimated the suitable length of the combustion chamber. Kindaracki et al. (2009) and Lu et al. (2010) also experimentally studied this topic. For the numerical approach, Hishida et al. (2009) estimated the detailed shock structure of the rotating detonation. Yi et al. (2010) simulated a RDE with exhaust nozzles to show the potential of new propulsive engines. Yamada et al. (2010) also simulated the 2D RDE to understand the mechanism of the transverse wave, which is required for continuous detonation. Nordeen et al. (2011) and Schwer and Kailasanath (2010, 2011) simulated a RDE in a hydrogen/air mixture. Zhou and Wang (2012) simulated a hydrogen/oxygen RDE, but they did not show the Isp value. The authors simulated the 3D RDE to show that the RDE had a larger Isp than the conventional rocket engine. Tsuboi et al. (2015) simulated a RDE in a hydrogen/oxygen mixture. The authors simulated the effects of the dimensions, grid resolution, scale, and stagnation pressure on the internal flow structure and thrust performance.

Recently, a RDE with a nozzle has been studied to improve the thrust performance. Rankin et al. (2014) experimentally studied a RDE with a converging-diverging (CD) nozzle to reduce the oscillation in the exhaust flow. The requirement for this reduction is because the exhaust oscillation is one of the major disadvantages for a gas turbine engine. However, there are many unclear phenomena, such as the details of the flow structure in the internal flow, effect of the nozzle geometry, and effects of the mass flow ratio on the thrust performance. In the present study, a 3D simulation for a RDE with a CD nozzle is performed to determine the effect of the nozzle geometry on the thrust performance, exhaust oscillation, and detailed internal flow.

Numerical method and physical model

Numerical method

The governing equations are the 3D Euler equations with a detailed chemical reaction model. Euler equations are commonly used in numerical calculations of detonation waves because the large scales generated by the shock wave are not always affected by viscous effects (Oran et al., 1998). In this study, the effect of the viscosity, thermal condition, and mass diffusion are assumed to be negligible. The governing equations include the mass conservation of nine species (H_2, O_2, O, H, OH, HO_2, H_2O_2, H_2O, N_2) and are summarized as follows:

$$\frac{\partial \boldsymbol{Q}}{\partial t} + \frac{\partial \boldsymbol{E}}{\partial \mathrm{x}} + \frac{\partial \boldsymbol{F}}{\partial y} + \frac{\partial \boldsymbol{G}}{\partial z} = \boldsymbol{S} \tag{1}$$

$$\boldsymbol{Q}=\begin{pmatrix}\rho\\ \rho u\\ \rho v\\ \rho w\\ e\\ \rho_i\end{pmatrix}\boldsymbol{E}=\begin{pmatrix}\rho u\\ \rho u^2+\rho\\ \rho uv\\ \rho uw\\ u(p+e)\\ \rho_i u\end{pmatrix}\boldsymbol{F}=\begin{pmatrix}\rho v\\ pvu\\ \rho v^2+\rho\\ \rho vw\\ v(p+e)\\ \rho_i v\end{pmatrix}$$
$$\boldsymbol{G}=\begin{pmatrix}\rho w\\ \rho wu\\ \rho wv\\ \rho w^2+P\\ w(p+e)\\ \rho_i w\end{pmatrix}\boldsymbol{S}=\begin{pmatrix}0\\ 0\\ 0\\ 0\\ 0\\ \dot{\omega}_i\end{pmatrix} \tag{2}$$

The pressure p, total energy e, and production rate $\dot{\omega}_i$ of the ith species by the chemical reaction $\dot{\omega}_i$ are calculated as:

$$p=\sum_{i=1}^{N_s}\rho_i R_i T_i \tag{4}$$

$$e=\sum_{i=1}^{N_s}\rho_i h_i-p+\frac{1}{2}\rho u^2+\frac{1}{2}\rho v^2+\frac{1}{2}\rho w^2 \tag{5}$$

$$w_i=W_i\sum_{k=1}^{N_r}\left(\upsilon_{ik}^{''}-\upsilon_{ik}^{'}\right)\left\{k_{f,k}\prod_{i=1}^{N_s}c_{x_i}^{\upsilon_{ik}^{'}}-k_{b,k}\prod_{i=1}^{N_s}c_{x_i}^{\upsilon_{ik}^{''}}\right\} \tag{6}$$

where N_s is the total number of species, ρ is the density, R is the gas constant, T is the temperature, v' are the stoichiometric coefficients of the reactants, v'' are the stoichiometric coefficients of the products, W_i is the molecular weight, N_r is the total number of elementary reactions, k_f is the forward specific reaction-rate constant, k_b is the backward specific reaction-rate constant, and c_x is the concentration.

Because the temperature in the detonations increases to more than 4000 K, the specific heat C_{pi} at constant pressure, enthalpy h_i, and entropy S_i of each chemical species (i = 1, 2, 3,…, N) depend on the temperature as follows:

$$\frac{C_{pi}}{R_i}=a_{1i}+a_{2i}T+a_{3i}T^2+a_{4i}T^3+a_{5\mathrm{i}}T^4 \tag{7}$$

$$\frac{h_i}{R_i T}=a_{1i}+\frac{a_{2i}}{2}T+\frac{a_{3i}}{3}T^2+\frac{a_{4i}}{4}T^3+\frac{a_{5\mathrm{i}}}{5}T^4+\frac{a_{6i}}{T} \tag{8}$$

$$\frac{S_i^0}{R_i}=a_{1i}\ln T+a_{2i}T+\frac{a_{3i}}{2}T^2+\frac{a_{4i}}{3}T^3+\frac{a_{5\mathrm{i}}}{4}T^4+a_{7i} \tag{9}$$

The coefficients $a_{1i,}a_{2i,}\ldots a_{7i}$ of each species are provided in the JANNAF table. A second-order AUSMDV (Wada and Liou, 1994) is used for the numerical flux in the convective terms. In the time integration, the third-order TVD Runge–Kutta method is applied. The

UT-JAXA (Shimizu et al., 2011) model is used for the chemical kinetics to solve the detonation problems. The chemical reaction source terms are treated in a linearly point-implicit manner to avoid the stiffness problem.

Physical model

The physical model of RDE is shown in Figure 1 for a coaxial chamber. In this study, the calculation domain of the 3D simulation is the RDE coaxial chamber, which is attached to the CD nozzle. The 1D detonation results are passed along the circumferential direction to start the rotating detonation.

In fact, the head end is drilled with a large number of micro laval nozzles or slits to inject a premixed stoichiometric H_2/O_2 gas mixture into the chamber. In the simulation, there are four boundary condition systems for the mixture injection:

(1) If the inlet pressure is significantly high, gas injection is impossible. The pressure on the side of the combustion chamber is assigned to be the pressure on the side of the nozzle, and the injection velocity is zero.
(2) If the inlet pressure is high, the gas injects at subsonic velocity without choking. The pressure on the combustion chamber side is assigned as the pressure on the nozzle side.
(3) If the inlet pressure is relatively high, the shock wave occurs in the nozzle and injects at subsonic velocity. The pressure on the combustion chamber side is assigned as the pressure on the nozzle side.
(4) If the inlet pressure is notably low, the gas accelerates in the expansion region and injects at supersonic velocity. The injection is not affected by the wall pressure. The reactant is injected at supersonic velocity.

The outlet boundary conditions are provided at the exit of the RDE using two patterns, but the flow cannot go backwards from the downstream to the upstream.

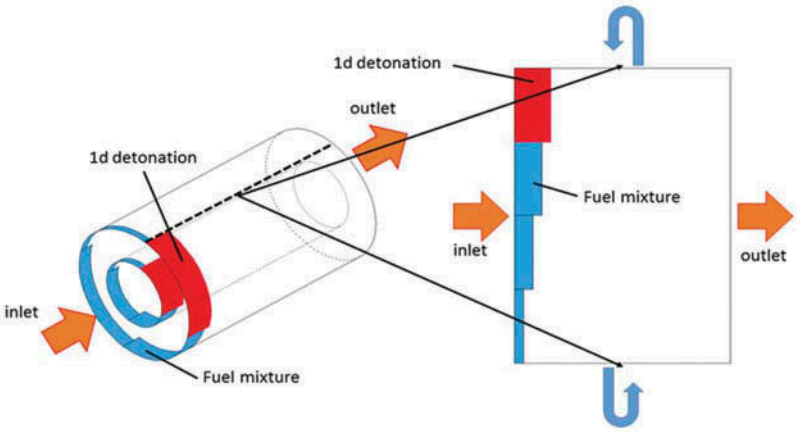

Figure 1. Modeling of the 3D RDE.

(1) The exit pressure of the RDE is assigned ambient pressure when the exhaust gas velocity is subsonic.
(2) The exit pressure of the RDE is assigned the values in the combustion chamber when the exhaust gas velocity is supersonic.

Grid system and simulation condition

The 3D grid system of the RDE with a CD nozzle is shown in Figure 2. In this study, the calculation grids are prepared with two patterns: Figure 2a shows a RDE with a throat and Figure 2b shows a RDE without a throat. In this article, (a) and (b) are defined as nozzles A and B, respectively. The expansion area ratios of nozzles A and B are 2.0 and 1.89, respectively. Figure 3 shows the cross-section area of nozzles A and B along the axial direction. The red line represents the throat part. The computational grid points are 241 (axial) × 11 (radial) × 601 (circumferential). The minimum grid widths near the rotating detonation area are 5 μm for the axial direction, 9.4 μm for the radial direction, and 3.93 and 4.95 μm for the inner and outer circumferential directions, respectively. Therefore, the radius ratio R_{outer}/R_{inner} is 1.25. The fine grid system is used near the rotating detonation head, and the coarse grid system is used in another region. The nozzle geometry is designed based on the nozzle in the reference of Rankin et al. (2014). The nozzle consists of a long constant cross-section area, a short converging section, and a diverging section.

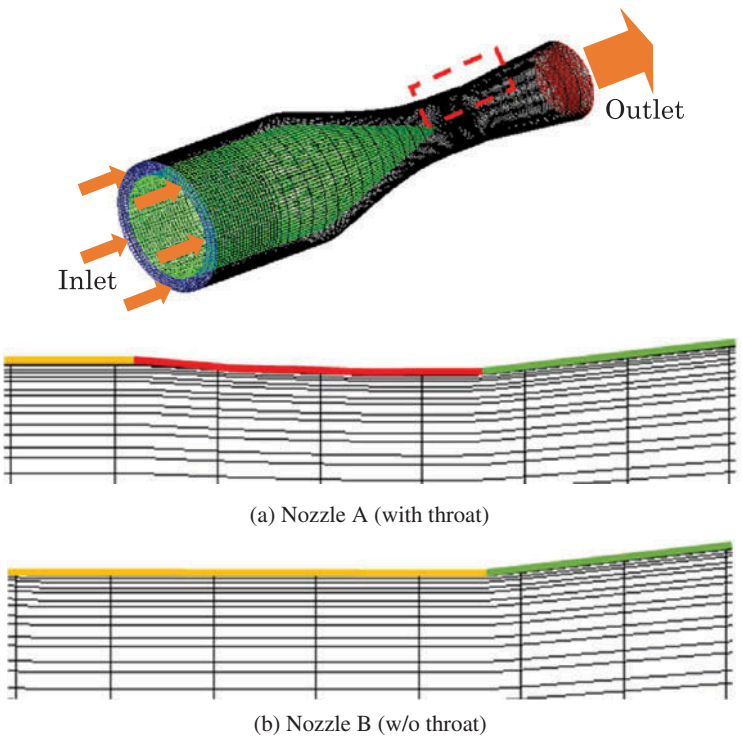

(a) Nozzle A (with throat)

(b) Nozzle B (w/o throat)

Figure 2. 3D grid of the RDE with a C-D nozzle (241 × 11 × 601).

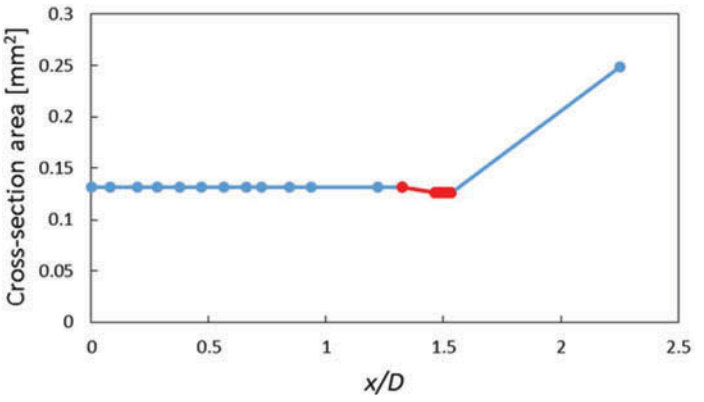

(a) Nozzle A (with throat)

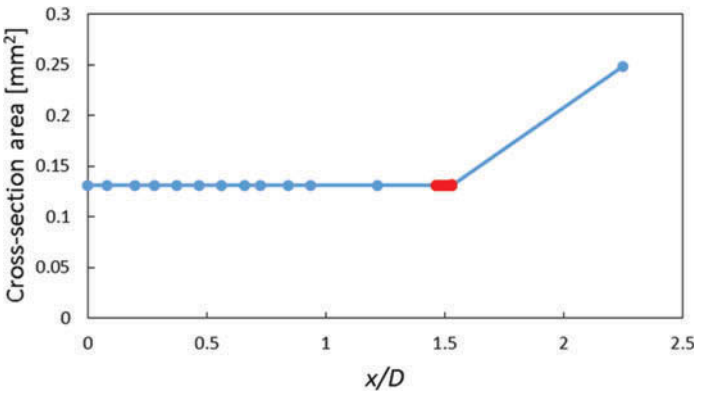

(b) Nozzle B (w/o throat)

Figure 3. Cross-section area along the axial direction.

In the diverging nozzle section, the area ratio of the exit to the throat is 1.98 to produce a supersonic flow under isentropic conditions. The Mach number of the supersonic flow region is approximately 2.2.

The ambient conditions are the conditions behind the nozzle. The ambient pressure p_e is 0.01 MPa, and the ambient temperature is 300 K. The pressure P_0 and temperature T_0 in the stagnation chamber are 2–5 MPa and 300 K, respectively. The micro-nozzle area ratio of the throat to the nozzle exit at the injection port (A^*/A) is 0.1. The stoichiometric H_2/O_2 gas mixture is supplied through the micro-nozzles.

Results and discussion

Effect of the throat on the exhaust oscillation

Figure 4 shows the flow structure in the RDE with a nozzle in this study. Figure 5 shows the time history of the averaged pressure at the nozzle exit section. The exhaust oscillation decreases with the CD nozzle, as shown in Figure 5. Figures 5a and 5b show the cases of nozzles A and B, respectively. The variation of the time-averaged pressure in Figure 5a is approximately 0.0048 MPa, and the ratio to the time-averaged value

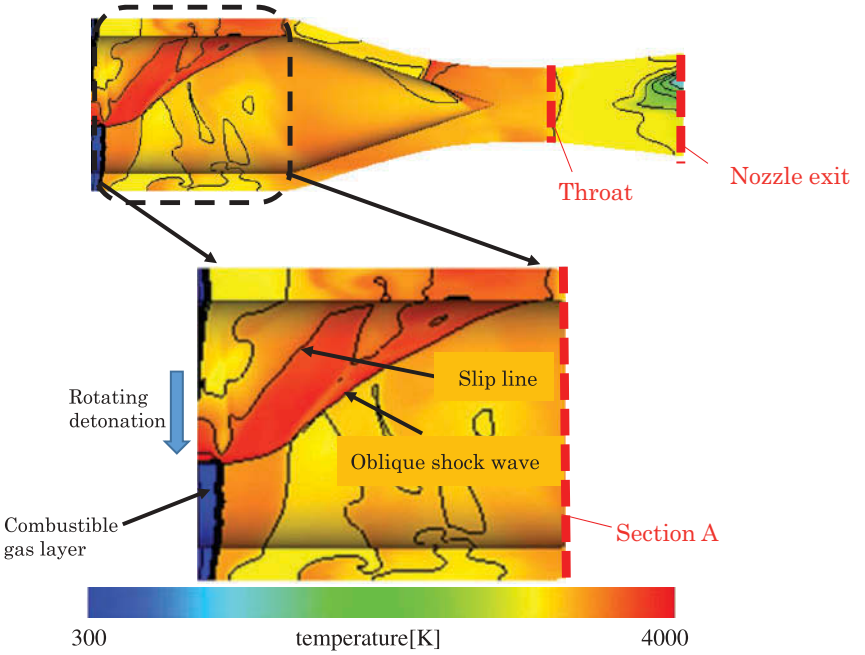

Figure 4. Flow structure in the 3D RDE.

(approximately 0.38 MPa) is 1.3%. The variation in Figure 5b is approximately 0.018 MPa, and the ratio to the time-averaged value (approximately 0.36 MPa) is 5%. These values are shown in Table 1. This result occurs because the flow is choked at the throat of the CD nozzle. Thus, the present CD nozzle can reduce the exhaust oscillation, as shown in Tsuboi et al. (2015).

Figure 6 shows the instantaneous Mach contours at various sections with three types of RDEs. The positions of section A, throat, and nozzle exit are indicated in Figure 4. The chamber exit is represented as section A. At section A, the averaged Mach number becomes subsonic for the RDE with a CD nozzle and supersonic for the RDE without a CD nozzle. At the throat section, there are different Mach number contours between nozzles A and B. For nozzle A, the internal flow does not become supersonic. The internal flow Mach number is uniformly distributed in the cross section. For nozzle B, the internal flow becomes supersonic, and the Mach number is nonuniform in the cross section. In other words, there is no shock wave at the nozzle throat in the case of nozzle A. The shock wave is assumed to disappear in the conversing nozzle region. At the nozzle exit, the Mach number becomes supersonic in both nozzles. There are discussions regarding the flow features at the front of the throat in the section, "Time-averaged flow field." Figure 7 shows the instantaneous Mach number contours of the RDE with a nozzle. From Figure 7, the Mach number of the internal flow is assumed to become subsonic near the detonation propagation region in the case without the nozzle. Another region becomes supersonic. In the case of nozzle A, the Mach number in most regions, except the divergent region, becomes subsonic.

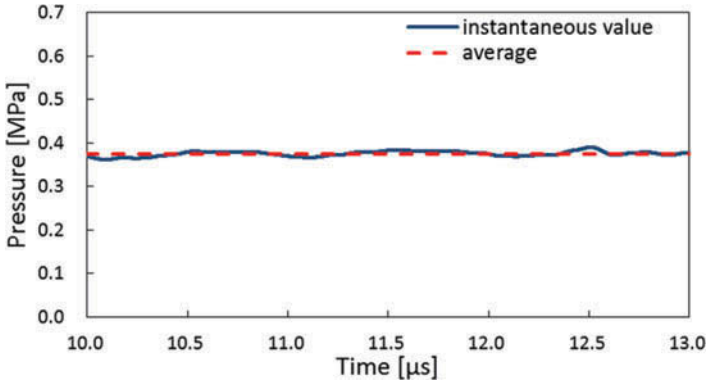

(a) Nozzle A (with throat).

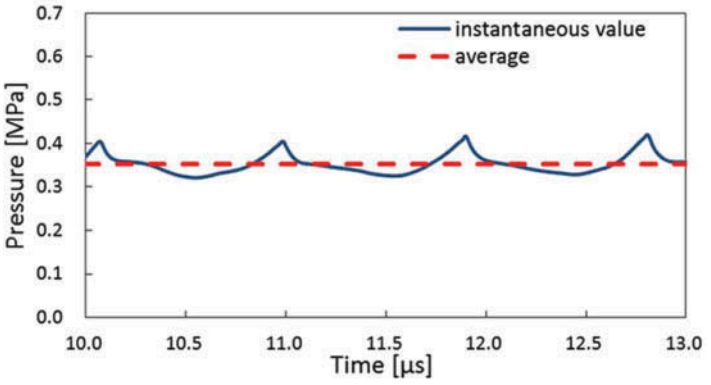

(b) Nozzle B (w/o throat).

Figure 5. Time history of the pressure at the nozzle exit.

Table 1. Time-averaged pressure and time-averaged variation.

	Nozzle A	Nozzle B
Average	0.38 (MPa)	0.36 (MPa)
Variation	0.0048 (MPa) (1.3%)	0.018 (MPa) (5%)

Effect of the contraction on the Isp

Figure 8a compares the average Isp of five cycles in the steady state between the cases of nozzles A and B. This figure shows that Isp is independent of the stagnation pressure. The specific impulse of nozzle A is approximately 11 s (3.8%) longer than that of nozzle B. Figure 8b compares the time-averaged thrust, which is calculated by averaging five cycles during the steady state. Figure 8c compares the time-averaged injected mixture per time. The time-averaged thrust of nozzle A is approximately 51,000 N/m^2 (3.7%) larger than that of nozzle B. Because there is a small difference in injected mixture per time, the difference in Isp is assumed to result from the difference in time-averaged thrust. Therefore, the throat shape affects the thrust performance. The comparison with experiments is necessary to validate this calculation in the future.

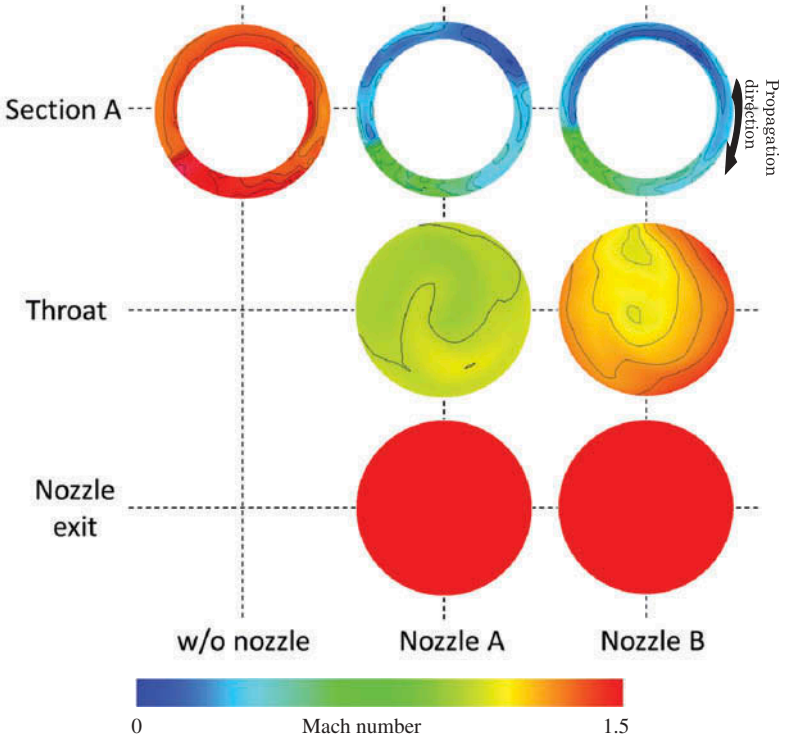

Figure 6. Instantaneous Mach contours at various sections.

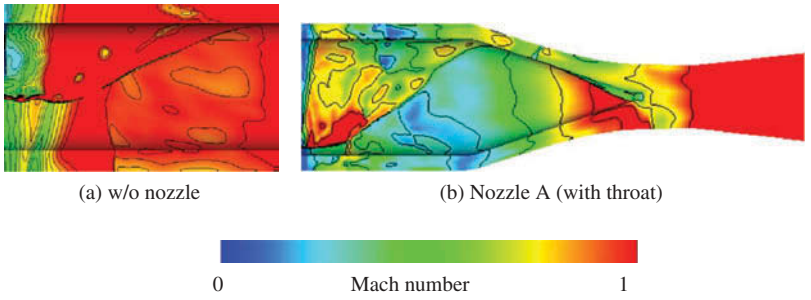

Figure 7. Effect of the nozzle on the Mach number contours in the RDE.

Time-averaged flow field

Figure 9 shows the time-averaged Mach number contours. Figures 9a and 9b show the cases of the RDE with nozzles A and B, respectively. There are different contours near the throat. However, there is almost no difference in Mach number at another region. For nozzle A, the Mach number rapidly increases near the throat, whereas for nozzle B, the Mach number gradually increases in front of the throat.

Figure 10 shows the time-averaged Mach number distributions along the axial direction on the outer walls. The red line represents the throat part. The blue line represents the sonic line. In the combustion chamber, the Mach number decreases along the axial

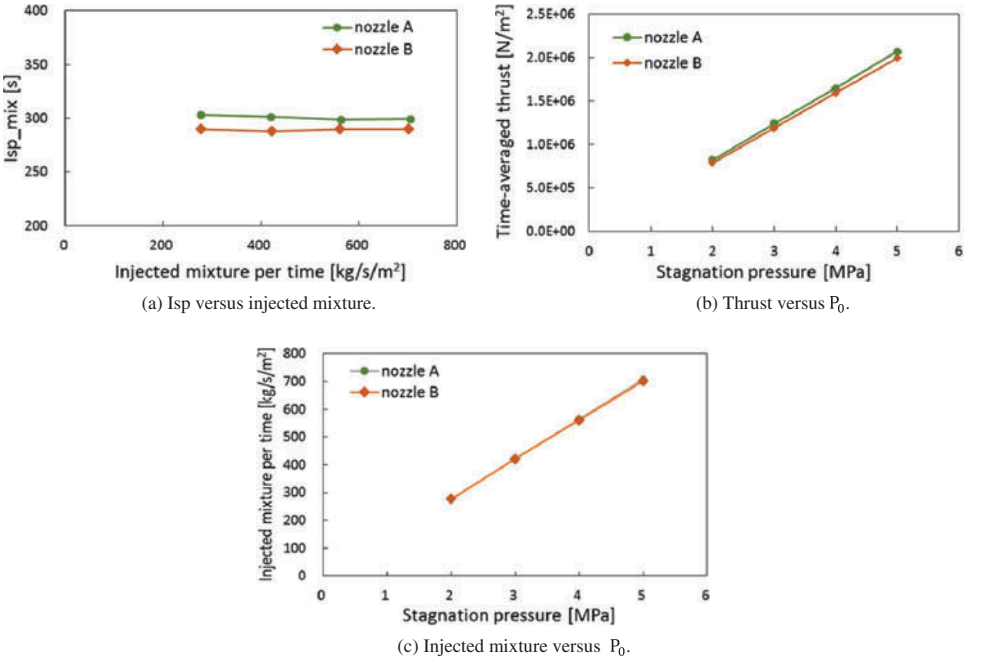

(a) Isp versus injected mixture.

(b) Thrust versus P_0.

(c) Injected mixture versus P_0.

Figure 8. Effect of the throat shape on the thrust performance.

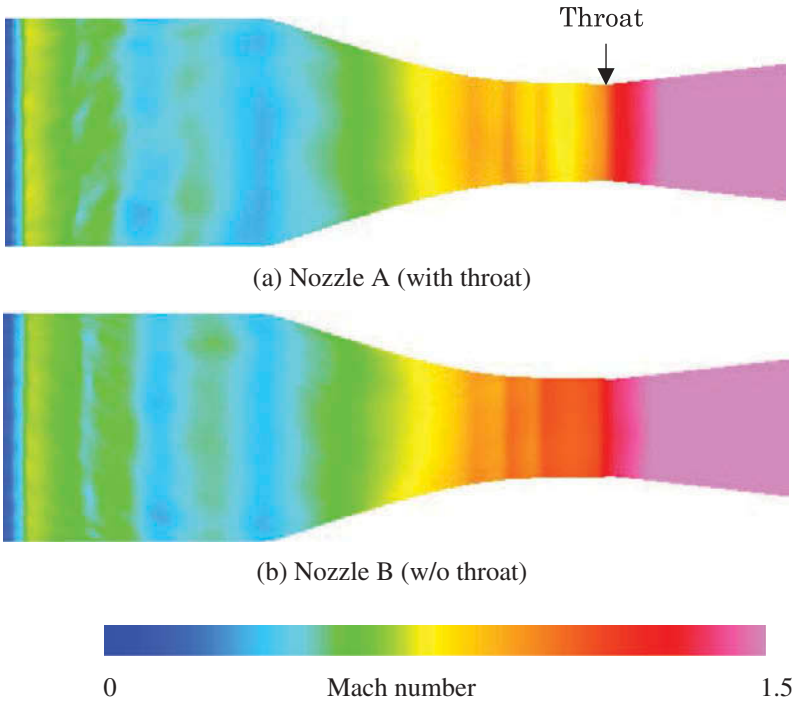

Figure 9. Time-averaged Mach number contours on the outer wall.

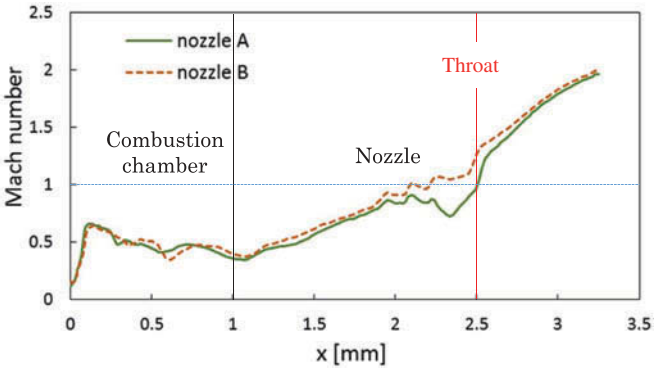

Figure 10. Time-averaged Mach number distribution along the axial direction (outer wall).

direction for x = 0.2 mm and 1.2 mm. The Mach number decreases at x = 2.0–2.35 mm and becomes supersonic at the throat for nozzle A, whereas it increases to become supersonic in the identical region for nozzle B. Both nozzles have similar nozzle exit Mach numbers of approximately 2.0.

Conclusions

A 3D numerical simulation of the 3D RDE with the CD nozzle is performed using the H_2/O_2 detailed chemistry model. The conclusions are as follows:

- The CD nozzle reduces the pressure oscillation at the nozzle exit. For nozzle A, the variation of the time-averaged pressure is approximately 0.0048 MPa and the ratio to the time-averaged value (approximately 0.38 MPa) is 1.3%. For nozzle B, the variation in pressure is approximately 0.018 MPa and the ratio to the time-averaged value (approximately 0.36 MPa) is 5%. For nozzle A, the internal-flow Mach number is uniformly distributed in the cross section. Therefore, the shock wave is assumed to disappear in front of the throat.
- The specific impulse of nozzle A is approximately 11 s (3.8%) longer than that of nozzle B. The time-averaged thrust of nozzle A is approximately 51,000 N/m^2 (3.7%) larger than that of nozzle B. The throat shape affects the thrust performance. The difference in Isp is assumed to result from the difference in the time-averaged thrust.
- The Mach number decreases at x = 2.0–2.35 mm for nozzle A, whereas the Mach number for nozzle B increases to become supersonic in the identical region. The nozzles have similar exit Mach numbers of approximately 2.0.

Acknowledgment

This study was collaborated with Cybermedia Center in Osaka University.

References

Hishida, M., Fujiwara, T., and Worlanski, P. 2009. Fundamentals of rotating detonations. *Shock Waves*, **19**, 1–10.

Kindaracki, J., Wolanski, P., and Gut, Z. 2009. Experimental research on the rotating detonation in gaseous fuels-oxygen mixtures. Presented at the 22nd ICDERS, Minsk, Belarus, July 27–31.

Lu, F.K., Dunn, N.L., and Braun, E.M. 2010. Testing of a continuous detonation wave engine with swirled injection. AIAA Paper 2010-146. Presented at the 48th AIAA Aerospace Sciences Meeting, Orlando, FL, January 4–7.

Nicholls, J.A., Cullen, R.E., and Ragland, K.W. 1966. Feasibility studies of a rotating detonation wave rocket motor. *J. Spacecraft Rockets*, **3**(6), 893–898.

Nordeen, C.A., Schwer, D., Schauer, F., Hoke, J., Cetegen, B., and Barber, T. 2011. Thermodynamic modeling of a rotating detonation engine. AIAA Paper 2011-0803. Presented at the 49th AIAA Aerospace Sciences Meeting, Orlando, FL, January 4–7.

Oran, E.S.,Weber, J.W., Stefaniw, E.I., Lefebvre, M.H., and Anderson, J.D. 1998. A numerical study of a two-dimensional H_2-O_2-air detonation using a detailed chemical reaction model. *Combust. Flame*, **113**, 147–163.

Rankin, B.A., Hoke, J.L., and Schauer, F.R. 2014. Periodic exhaust flow through a converging-diverging nozzle downstream of a rotating detonation engine. AIAA Paper 2014-1015. Presented at the 52nd AIAA Aerospace Science Meeting, National Harbor, MD, January 13–17.

Schwer, D.A., and Kailasanath, K. 2010. Numerical investigation of rotating detonation engines. AIAA Paper 2010-6880. Presented at the 46th AIAA/ASME/SAE/ASEE Joint Propulsion Conference, Nashville, Tennessee, July 25–28.

Schwer, D.A., and Kailasanath, K. 2011. Numerical study of the effects of engine size on rotating detonation engines. AIAA Paper 2011-581. Presented at the 49th AIAA Aerospace Sciences Meeting, Orlando, FL, January 4–7.

Shimizu, K., Hibi, A., Koshi, M., Morii, Y., and Tsuboi, N. 2011. Updated kinetic mechanism for high-pressure hydrogen combustion. *J. Propul. Power*, **27**(2), 383–395.

Tsuboi, N., Watanabe, Y., Kojima, T., and Hayashi, A.K. 2015. Estimation of the thrust performance on a rotating detonation engine for a hydrogen-oxygen mixture. *Proc. Combust. Inst.*, **35**, 2005–2013.

Voitsekhovskii, B.V. 1959. Stationary detonation. *Doklady Akad. Nauk USSR*, **129**(6), 1254–1256.

Wada, Y., and Liou, M.S. 1994. A flux splitting scheme with high-resolution and robustness for discontinuities. AIAA Paper 94-0083. Presented at the 32nd AIAA Aerospace Sciences Meeting, Reno, NV, January 10–13.

Wolanski, P. 2013. Detonation propulsion. *Proc. Combust. Inst*, **34**, 125–158.

Yamada, T., Hayashi, A.K., Yamada, E., Tsuboi, N., Tangirala, V.E., and Fujiwara, T. 2010. Detonation limit thresholds in H_2/O_2 rotating detonation engine. *Combust. Sci. Technol.*, **182** (11–12), 1901–1914.

Yi, T.H., Lou, J., Turangan, C., Khoo, B.C., and Wolanski, P. 2010. Effect of nozzle shapes on the performance of continuously rotating detonation engine. AIAA paper 2010-152. Presented at the 48th AIAA Aerospace Sciences Meeting, Orlando, FL, January 4–7.

Zhdan, S.A., Bykovskii, F.A., and Vedernikov, E.F. 2007. Mathematical modeling of a rotating detonation wave in a hydrogen–oxygen mixture. *Combust. Explos. Shock Waves*, **43**(4), 449–459.

Zhou, R., and Wang, J.-P. 2012. Numerical investigation of flow particle paths and thermodynamic performance of continuously rotating detonation engines. *Combust. Flame*, **159**(12), 3632–3645.